IEEE Access
Multidisciplinary | Rapid Review | Open Access Journal

Received May 13, 2021, accepted May 24, 2021, date of publication May 27, 2021, date of current version June 8, 2021.

Digital Object Identifier 10.1109/ACCESS.2021.3084285

Compound Metaloop Antenna for Circularly Polarized Beam Steering

HISAMATSU NAKANO, (Life Fellow, IEEE), TOMOKI ABE, (Member, IEEE), AND JUNJI YAMAUCHI, (Life Fellow, IEEE)
Science and Engineering, Hosei University, Koganei 184-8584, Japan

Corresponding author: Hisamatsu Nakano (hymat@hosei.ac.jp)

This work was supported in part by the Japan Society for the Promotion of Science (JSPS) KAKENHI under Grant JP21K04068.

ABSTRACT A metaloop antenna (1FD-MetaLPA), made of *C*-type metaatoms and having a single feed point, F_L', is created to radiate a left-hand circularly polarized (LHCP) axial beam at a frequency of $f_{LH-1FD} = 2.55$ GHz and a right-hand circularly polarized (RHCP) axial beam at a frequency of $f_{RH-1FD} = 3.45$ GHz. It is revealed that the maximum gains at f_{LH-1FD} and f_{RH-1FD} are unbalanced. Subsequently, a number of *C*-type metaatoms are replaced by *N*-type metaatoms. The replacement generates a balanced gain of 7.1 dBi with an LHCP gain bandwidth of 7.7% and an RHCP gain bandwidth of 8.3%. The radiation efficiency under the balanced gain is 75% at f_{LH-1FD} and 29% at f_{RH-1FD}. Next, a large metaloop antenna that radiates a conical beam and has a feed point, F_O, is concentrically added to the outside of the gain-balanced 1FD-MetaLPA. This antenna system is designated as the MetaLPA-plus. It is found that the MetaLPA-plus radiates an LHCP tilted beam at f_{LH-1FD} and an RHCP tilted beam at f_{RH-1FD}. The angle of depression (tilt angle) using equal amplitude excitation is $\theta_{max} = 20°$ at f_{LH-1FD} and $\theta_{max} = 15°$ at f_{RH-1FD}. These tilted CP radiation beams are rotated around the antenna axis with change in the excitation phases at points F_L' and F_O. During the beam-steering, the gain for an LHCP wave is nearly constant, with a value between 5 dBi and 6.5 dBi. This also holds true for an RHCP wave.

INDEX TERMS Circularly polarized wave, dual band operation, loop antenna, metaatoms, steerable beam.

I. INTRODUCTION

A loop antenna, abbreviated as LPAnT, is a resonant antenna and radiates a linearly polarized (LP) wave [1], [2]. It is found that when the loop length is one guided wavelength ($1\lambda_g$), an LPAnT located in the x-y plane forms an axial beam within the $\pm$z hemispheres. It is also found that an LPAnT of length $2\lambda_g$ forms a conical beam within the $\pm$z hemispheres. These axial and conical beams can be changed into radiation beams within the +z hemisphere by using a conducting plane reflector placed under the loop. Conventionally, the distance between the reflector and the loop is set to be one-quarter wavelength ($\lambda_0/4$ with λ_0 being the free-space wavelength) to realize in-phase field superimposition, where the radiation reflected by the reflector is constructively superimposed within the +z hemisphere onto the direct radiation from the LPAnT.

Literature [3] reveals that the LP beam from the $1\lambda_g$ LPAnT can be changed into a circularly polarized (CP) beam by adding perturbation elements to the loop. This technique is applied to generation of CP beams in [4], [5]. These CP beams have unidirectional radiation using a conducting reflector, with distances from the loop to the reflector being $\lambda_0/4$ [4] and $\lambda_0/8$ [5].

With the emergence of metamaterials, new *line* antennas based on a composite right- and left-hand transmission line have been proposed [6]–[10]. These antennas, classified as metaline antennas, are composed of subwavelength cells (*C*-type metaatoms), with each cell radiating an LP wave. As a result, the metaline antenna itself radiates an LP wave, where the antenna height above the ground plane is extremely small: on the order of $\lambda_0/100$.

Such a small antenna height is found for the square LPAnT in [11], where each side-arm is composed of a linear metaline. The square LPAnT radiates a CP wave. In addition, an antenna whose arm is composed of a curved metaline, designated as the round metaloop antenna, is also found to have a small antenna height and radiate a CP wave [12].

This paper presents an antenna system, abbreviated as the MetaLPA-plus, that is an application of the round

The associate editor coordinating the review of this manuscript and approving it for publication was Chan Hwang See.

metaloop antenna. The presented MetaLPA-plus has a low-profile structure (the antenna height is on the order of $\lambda_0/100$) and radiates a CP tilted beam that can be rotated (steered) around the antenna axis at two design frequencies. The tilted beam is left-hand circularly polarized (LHCP) at the low design frequency of $f_{\mathrm{LH-1FD}}$ and right-hand circularly polarized (RHCP) at the high design frequency of $f_{\mathrm{RH-1FD}}$. In other words, the MetaLPA-plus is an innovative antenna with an extremely low-profile structure that has a steerable dual-band counter CP tilted beam. These key characteristics are determined through simulations using a commercially available electromagnetic solver [13].

While polarization alignment is required between an LP transmitting antenna and the corresponding LP receiving antenna, it is not required for CP antennas. The direction of polarization for LP antennas attached to moving bodies (*e.g.*, drones, helicopters, airplanes, satellites, and land vehicles) changes with the movement of the moving body. In contrast, the MetaLPA-plus presented in this paper is a CP antenna and does not require polarization alignment; hence, it can be used on such moving bodies for dual-band communications, where the gain at $f_{\mathrm{LH-1FD}}$ and $f_{\mathrm{RH-1FD}}$ does not necessarily need to be the same.

In addition, it is emphasized that the MetaLPA-plus can be used as an anti-jamming/anti-interference antenna in, for example, satellite-to-satellite communications, satellite-to-base station communications, vehicle-to-vehicle communications, and vehicle-to-base station communications. When an LHCP communication link at $f_{\mathrm{LH-1FD}}$ is disturbed by jamming signals (an LHCP wave at $f_{\mathrm{LH-1FD}}$), the MetaLPA-plus can immediately provide another communication link with the opposite polarization (RHCP) at $f_{\mathrm{RH-1FD}}$ without introducing an additional antenna, because the MetaLPA-plus itself is a counter CP dual-band antenna. This feature can thus provide a countermeasure to signal jamming. In such a case, it is desired that the gain at $f_{\mathrm{LH-1FD}}$ is as close as possible to the gain at $f_{\mathrm{RH-1FD}}$, thereby facilitating the design of a communication system that involves power amplifiers. Note that even if the MetaLPA-plus has an unbalanced gain, it does not lose its anti-jamming/anti-interference capability. However, the design of communication systems with unbalanced gain is somewhat complicated, compared with that for balanced gain.

Table 3 is presented in the Appendix to provide a better understanding of the novelty/advantages of the MetaLPA-plus. It is clear that only the presented MetaLPA-plus has the features of counter CP and dual-band characteristics, with a small antenna height on the order of approximately $\lambda_0/100$.

II. ANTENNA GEOMETRY AND DESIGN CONCEPTS

A. 3FD-METALPA (STEP ONE)

Fig. 1 shows a metaloop antenna, MetaLPA$_{\mathrm{i}}$, where C-type metaatoms form a round loop structure. Point F_{i} is the feed point and point T_{i} is the terminal point, which is shorted through resistive load R_{B} (= 50 ohms) to a ground plane (GP). The parameters for the C-type metaatom are summarized in Table 1, where ε_{r} and B are the relative permittivity and thickness of the grounded dielectric substrate, respectively;

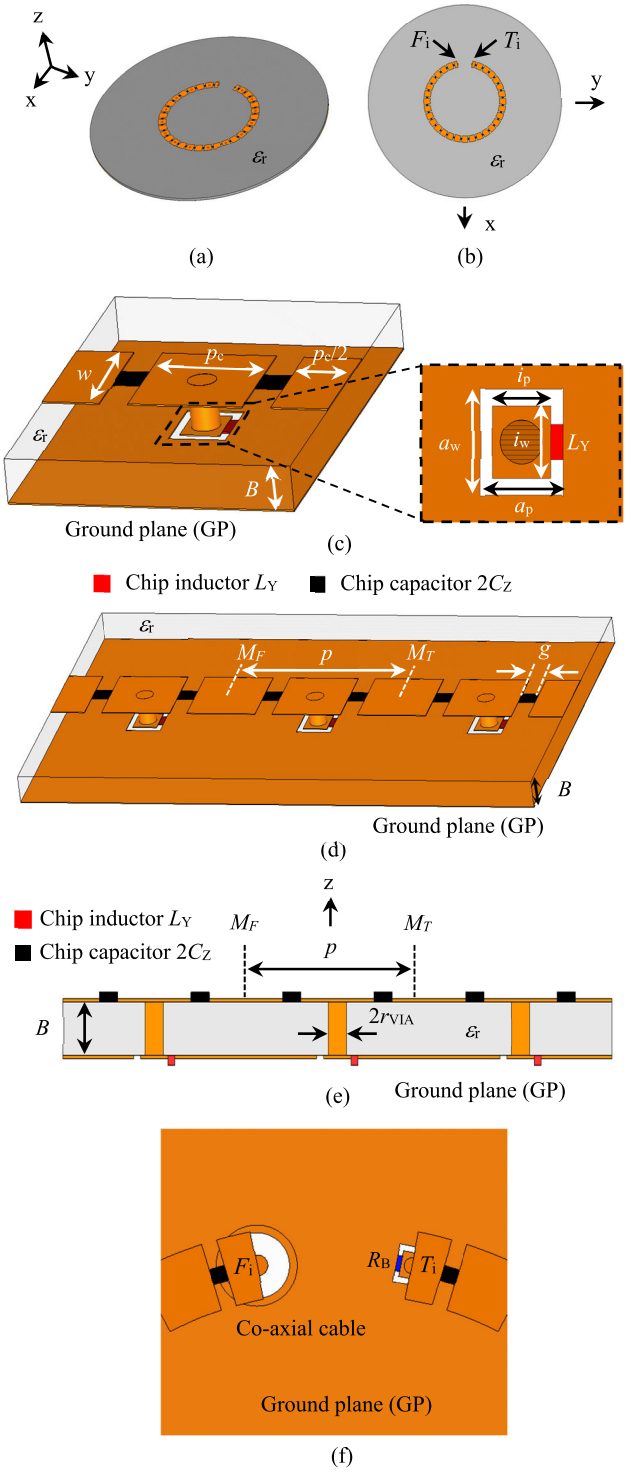

FIGURE 1. ***C*-type metaloop antenna. (a) Perspective view. (b) Top view. (c) *C*-type metaatom. (d) Connected *C*-type metaatoms. (e) Side view of the connected *C*-type metaatoms. (f) Feed point F_{i} excited by a co-axial cable. T_{i} is the terminal point shorted through resistive load R_{B} = 50 ohms to the ground plane. The gap/distance between the feed and terminal points is 10 mm. The first and last patches have a length of $p_{\mathrm{c}}/2$. A conducting pin is connected to every other strip (patch), while the remaining strips (patches) have no pin connected.**

TABLE 1. Parameters for the *C*-type metaatom.

Symbol	Value	Symbol	Value
B	1.6 mm	ε_r	2.6
p	10.0 mm	w	4.4 mm
p_c	4.0 mm	$2r_{via}$	1.0 mm
g	1.0 mm	L_Y	2.0 nH
$2C_Z$	1.4 pF	a_p	2.0 mm
a_w	2.45 mm	i_p	1.4 mm
i_w	1.65 mm		

$p = 2p_c + 2g$ is called the periodicity, with p_c being the length of a subwavelength strip/patch (Sub-STRP) and g being the gap between neighboring Sub-STRPs; r_{VIA} is the radius of a conducting pin (via) connecting the center point of the metaatom through a chip inductor, L_Y, to the ground plane. Note that neighboring Sub-STRPs are connected through chip capacitors, $2C_Z$.

The C-type metaatom can be represented by a four-port transmission line circuit expressed by series impedance Z and parallel admittance Y [6]. Z consists of the distributed inductance across the metaatom, the capacitance generated by the two gaps existing within the metaatom, and the two chip capacitors inserted into the gaps. Y consists of the distributed capacitance across the metaatom, the inductance generated by the vertical conducting pin, and the chip inductor inserted between the end of the conducting pin and the ground plane. The propagation phase constant of the current along the metaatom, $\beta(= 2\pi/\lambda_g$ with λ_g being the guided wavelength), is derived from $\sqrt{ZY}$, which shows $\beta = 0$ at frequency f_T (designated as the transition frequency), $\beta < 0$ at frequencies below f_T, and $\beta > 0$ at frequencies above f_T. The dispersion for the C-type metaatom is designed to have $f_T = 3$ GHz, as shown in Fig. 2, where k_0 $(= 2\pi/\lambda_0)$ is the wavenumber in free space. Note that the surface current on the C-type metaatom flows in the longitudinal direction (from M_F to M_T) and hence the radiation from the C-type metaatoms is linearly polarized.

Fig. 3 shows an antenna system composed of three metaloop antennas, the MetaLPA$_L$, MetaLPA$_M$, and MetaLPA$_S$, whose circumferences at the low design frequency of 2.55 GHz are $0.54\lambda_g$, $0.89\lambda_g$ and $1.24\lambda_g$, respectively. Points F_i (i = L, M, S) are the feed points and the diameter of the grounded substrate is $0.72\lambda_g$. The antenna system is designated as the 3FD-MetaLPA.

Each loop for the 3FD-MetaLPA at f_{LH-3FD} has a traveling wave current with a negative propagation phase constant ($\beta < 0$), resulting in generation of an LHCP radiation field of E_L; in contrast, each loop for the 3FD-MetaLPA at f_{RH-3FD} has a traveling wave current with a positive propagation phase constant ($\beta > 0$), resulting in generation of an RHCP radiation field of E_R. Fig. 4 shows the frequency response of the gain in the z-direction for the 3FD-MetaLPA, where the three metaloop antennas are excited in-phase. For comparison, the frequency response of the gain for a single (isolated) MetaLPA$_M$ is also shown in Fig. 4. Note that G_{LH} denotes the gain for a left-hand circularly polarized (LHCP) wave and G_{RH} denotes the gain for a right-hand circularly polarized (RHCP) wave. It is found that the maximum value of G_{LH} for the 3FD-MetaLPA is at f_{LH-3FD} ($\equiv 2.70$ GHz), which is below transition frequency f_T, and the maximum G_{RH} is at f_{RH-3FD} ($\equiv 3.35$ GHz), which is above f_T. It is found that the maximum gain for the 3FD-MetaLPA is only approximately 2 dB higher than that for the single (isolated) MetaLPA$_M$. It follows that using an array structure with three feed points has a small effect on the overall gain of the antenna system.

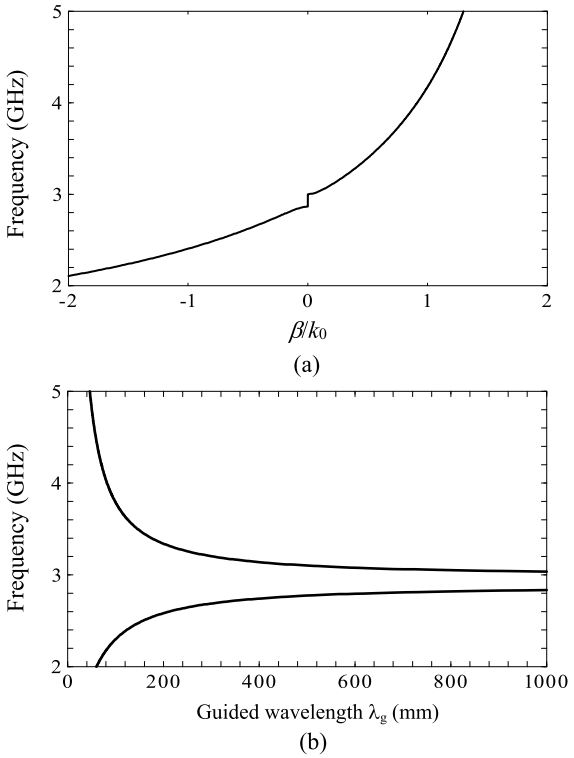

FIGURE 2. Dispersion of the *C*-type metaatom. (a) β/k_0 vs frequency. (b) Guided wavelength λ_g vs frequency.

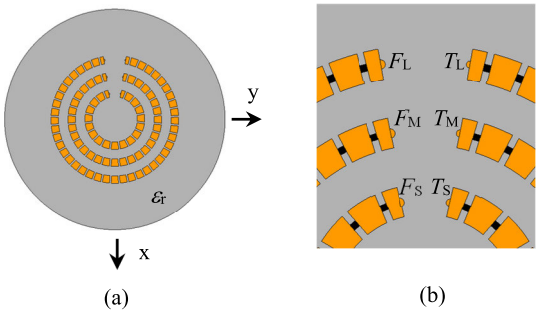

FIGURE 3. 3FD-MetaLPA composed of the MetaLPA$_L$, MetaLPA$_M$, and MetaLPA$_S$. (a) Top view. (b) Expanded view of the upper region.

B. 1FD-METALPA (STEP TWO)

We consider an antenna system that realizes a higher gain than that for the 3FD-MetaLPA. For this, three metaloop antennas, the MetaLPA$_L$, MetaLPA$_M$, and MetaLPA$_S$, are connected as

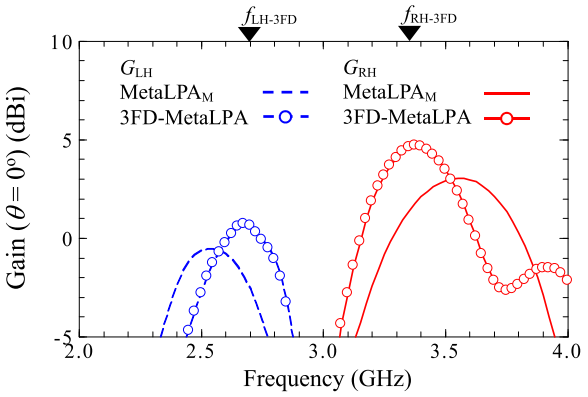

FIGURE 4. Frequency response of the gain for the 3FD-MetaLPA, together with that for reference MetaLPA$_M$.

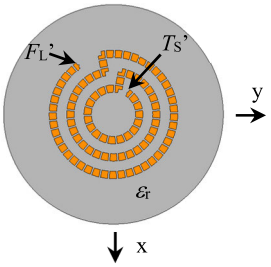

FIGURE 5. 1FD-MetaLPA with feed point F_L' and terminal point T_S', which is shorted to the ground plane through a resistive load.

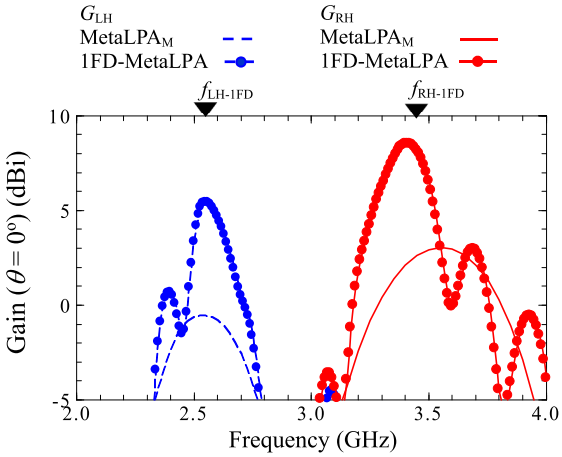

FIGURE 6. Frequency response of the gain for the 1FD-MetaLPA, together with that for the MetaLPA$_M$ reference.

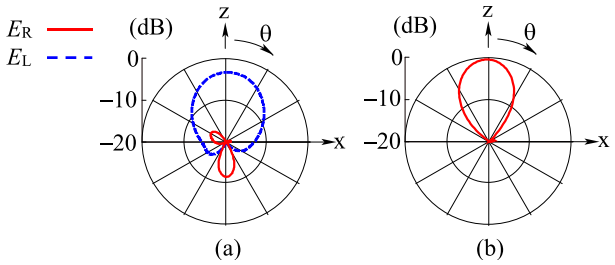

FIGURE 7. Radiation pattern for the 1FD-MetaLPA. (a) At f_{LH-1FD} = 2.55 GHz. (b) At f_{RH-1FD} = 3.45 GHz.

shown in Fig. 5, where point F_L' (close to the original F_L) is the feed point and point T_S' (close to the original T_S) is the terminal point, which is shorted to the ground plane through resistive load R_B (= 50 ohms). This antenna is designated as the 1FD-MetaLPA.

Fig. 6 shows the frequency response of the gain for the 1FD-MetaLPA, together with that for the MetaLPA$_M$ as a reference. It is revealed that the maximum value for G_{LH} is at 2.55 GHz ($\equiv f_{LH-1FD}$), and is 6.0 dB higher than that for the MetaLPA$_M$. In addition, the maximum value for G_{RH} is at 3.45 GHz ($\equiv f_{RH-1FD}$), and is 5.5 dB higher than that for the MetaLPA$_M$. Thus, a higher gain is obtained with the 1FD-MetaLPA than with the MetaLPA$_M$. The radiation patterns where G_{LH} and G_{RH} are at their maximum value are shown in Fig. 7.

C. GAIN BALANCING FOR 1FD-METALPA (STEP THREE)

Subsection *B* shows that the maximum value is increased for G_{LH} and G_{RH}, however, the left-hand and right-hand maximum gains are not balanced. In this section, these different maximum gains are adjusted to be balanced (nearly equal). For this, gain G_{LH} is increased using N-type metaatoms [10], based on the fact that the N-type metaatom radiates an LHCP wave.

The N-type metaatom is illustrated in Fig. 8, which is a modified version of the C-type metaatom shown in Fig. 1. For the N-type metaatom, the vertical conducting pin of the C-type metaatom (extending from the center strip through a chip inductor to the ground plane) is replaced by a stub of length l_{STB} and width w_{STB}. The stub extends to the right of the strip (patch), relative to the direction of the current flow from M_F to M_T, and is directly short-circuited to the ground plane without using a chip inductor. Thus, the stub generates part of parallel admittance Y in the four-port transmission line circuit representation. The current on the stub has a phase delay of 90 degrees relative to the phase of the surface current on the center strip. This generates LHCP radiation.

The dispersion for the N-type metaatom, as shown in Fig. 9, is designed to be as close as possible to the dispersion for the C-type metaatom shown in Fig. 2. The design parameters are summarized in Table 2.

Fig. 10 shows the change in the maximum gain values, G_{LH} at f_{LH-1FD} (= 2.55 GHz) and G_{RH} at f_{RH-1FD} (= 3.45 GHz), as a function of the number of N-type metaatoms, N_{atom}. It is found that there is an N_{atom} for which the maximum gain values are balanced on the 1FD-MetaLPA: N_{atom} = 15 $\equiv N_{GLH=GRH}$. The frequency response of the gain with

TABLE 2. Parameters for the N-type metaatom.

Symbol	Value	Symbol	Value
B	1.6 mm	ε_r	2.6
p	10.0 mm	w	4.4 mm
p_c	4.0 mm	$2r_{via}$	1.0 mm
g	1.0 mm	l_{STB}	7.2 mm
$2C_Z$	1.4 pF	w_{STB}	1.5 mm

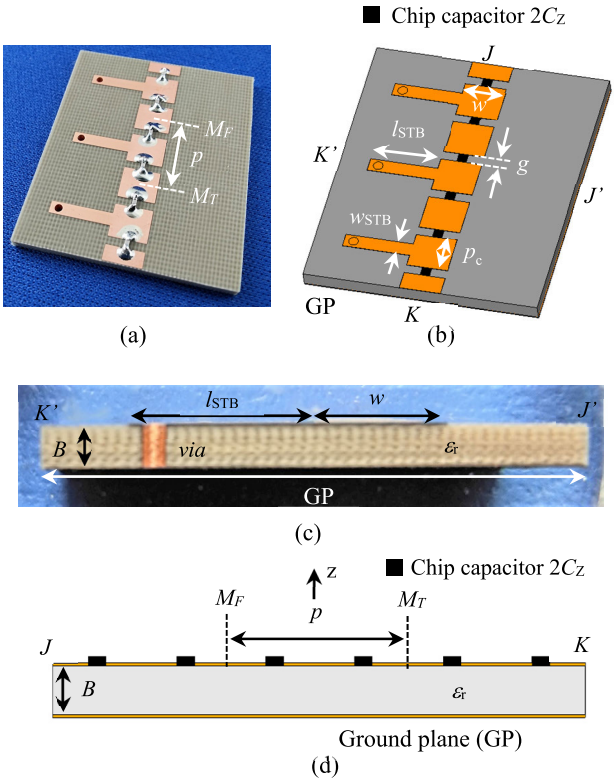

FIGURE 8. *N*-type metaatoms. (a) Photo of perspective view. A conducting pin/via is connected to every other strip/patch, while the remaining strips/patches have no pin/via connected. (b) Parameters. (c) Photo of cross section at line *J'K'*. (d) Cross section at line *JK*.

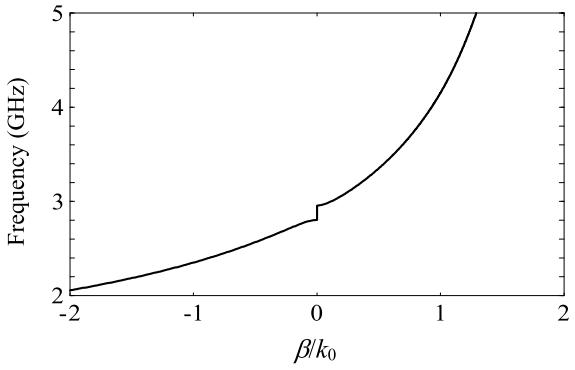

FIGURE 9. Dispersion of the *N*-type metaatom.

$N_{\mathrm{GLH=GRH}}$ is shown in Fig. 11(a). It is found that the 3-dB gain bandwidth is relatively wide: 7.7% for gain G_{LH} and 8.3% for gain G_{RH}. The radiation efficiency is 75% at $f_{\mathrm{LH-1FD}}$ and 29% at $f_{\mathrm{RH-1FD}}$, as shown in Fig. 11(b).

Comments on these radiation efficiencies are made here. The input power reaches the end of the antenna arm and is absorbed by resistive load R_{B} (= 50 ohms). The absorbed power is related to attenuation constant α of the propagation constant, which depends on the operating frequency. Our preliminary calculation shows that α has the following characteristic: $-\alpha$ at $f_{\mathrm{RH-1FD}} < -\alpha$ at $f_{\mathrm{LH-1FD}}$. This means that the attenuation per 1 m, $e^{-\alpha}$, at $f_{\mathrm{RH-1FD}}$ is smaller than that at $f_{\mathrm{LH-1FD}}$, and hence the absorbed power at $f_{\mathrm{RH-1FD}}$ is

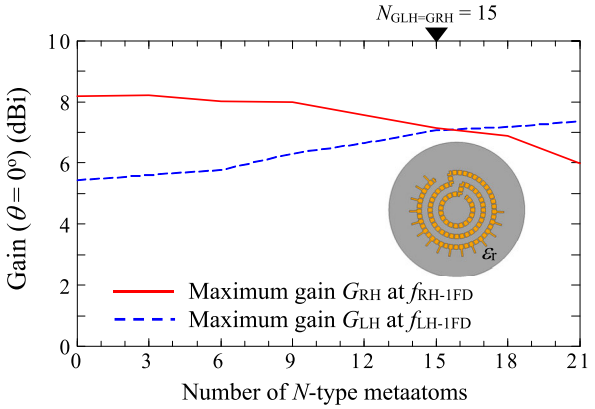

FIGURE 10. Maximum gain G_{LH} at $f_{\mathrm{LH-1FD}}$ = 2.55 GHz and G_{RH} at $f_{\mathrm{RH-1FD}}$ = 3.45 GHz as a function of the number of *N*-type metaatoms.

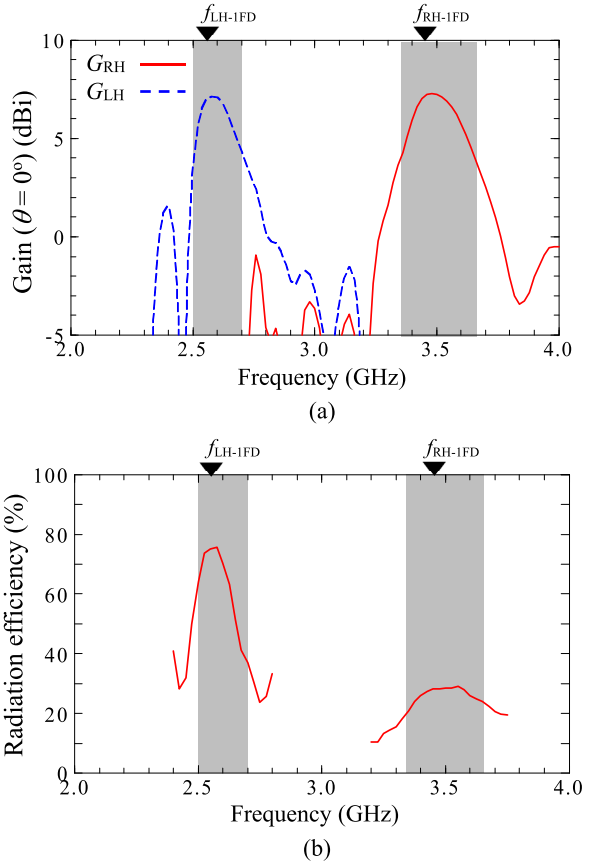

FIGURE 11. Frequency response. (a) Gain for the 1FD-MetaLPA with $N_{\mathrm{atom}} \equiv N_{\mathrm{GLH=GRH}}$. The shaded areas show 3-dB gain bandwidth regions. (b) Radiation efficiency.

larger than that at $f_{\mathrm{LH-1FD}}$. Thus, the input power transformed into radiation at $f_{\mathrm{RH-1FD}}$ is smaller than that at $f_{\mathrm{LH-1FD}}$. It follows that the radiation efficiency at $f_{\mathrm{RH-1FD}}$ is smaller than that at $f_{\mathrm{LH-1FD}}$. Note that, generally, the radiation efficiency is improved by increasing the thickness of the substrate.

Fig. 12 shows the radiation pattern when a balanced gain of 7.1 dBi is obtained at frequencies $f_{\mathrm{LH-1FD}}$ and $f_{\mathrm{RH-1FD}}$. The principal radiation field components around frequencies $f_{\mathrm{LH-1FD}}$ and $f_{\mathrm{RH-1FD}}$ are E_{L} and E_{R}, respectively; this is

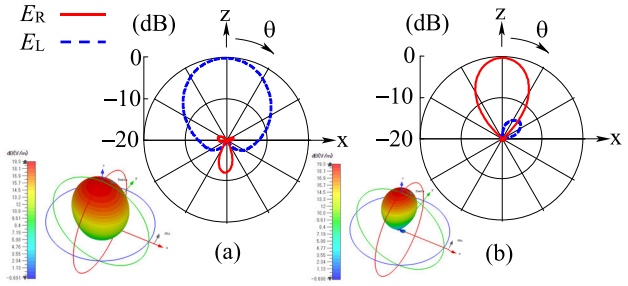

FIGURE 12. 2D and 3D radiation patterns for the gainbalanced 1FD-MetaLPA. (a) At $f_{\text{LH-1FD}} = 2.55$ GHz. (b) At $f_{\text{RH-1FD}} = 3.45$ GHz.

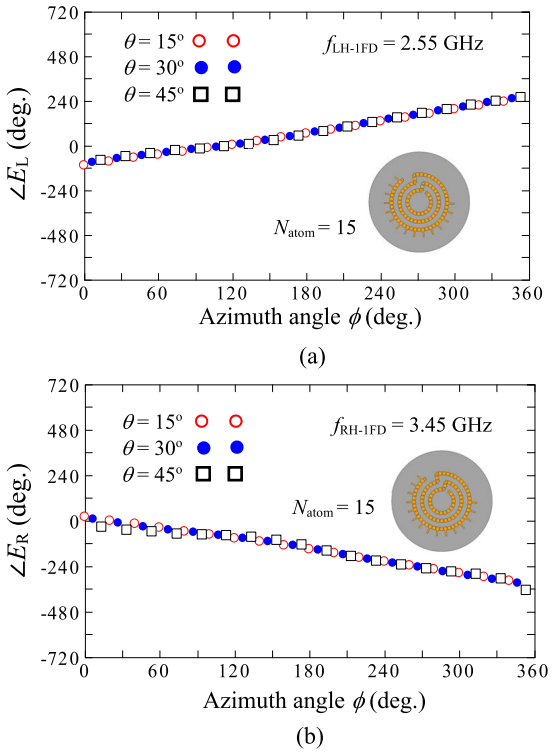

FIGURE 13. Phase as a function of azimuth angle ϕ with depression angle θ as a parameter. (a) $\angle E_L$ at $f_{\text{LH-1FD}} = 2.55$ GHz. (b) $\angle E_R$ at $f_{\text{RH-1FD}} = 3.45$ GHz.

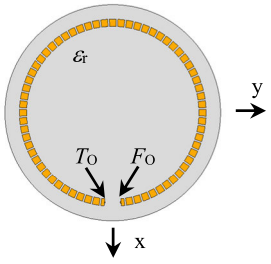

FIGURE 14. MetaLPA$_O$, where point F_O is the feed point and point T_O is the terminal point, which is short-circuited to the ground plane through a resistive load of 50 ohms.

consistent with the gain behavior. Fig. 13(a) depicts the phase progression for E_L at $f_{\text{LH}-1\text{FD}}$, which is progressive, and Fig. 13(b) depicts the phase progression for E_R at $f_{\text{RH}-1\text{FD}}$, which is regressive, both having a phase change of 360° in the azimuth direction.

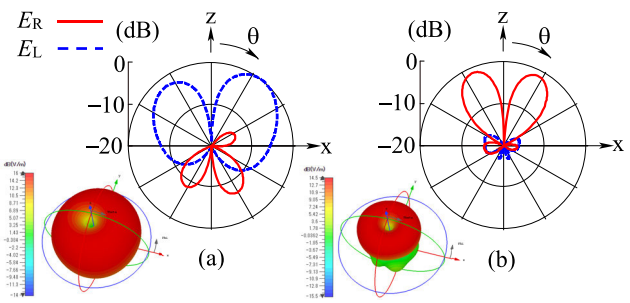

FIGURE 15. 2D and 3D radiation patterns for the MetaLPA$_O$. (a) At $f_{\text{LH}-1\text{FD}} = 2.55$ GHz. (b) At $f_{\text{RH}-1\text{FD}} = 3.45$ GHz.

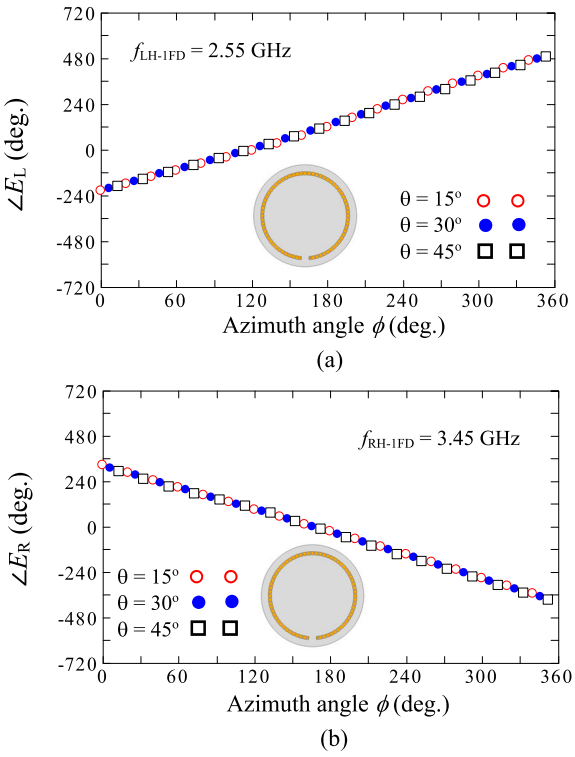

FIGURE 16. Phase of the radiation field from the MetaLPA$_O$. (a) $\angle E_L$ at $f_{\text{LH}-1\text{FD}}$. (b) $\angle E_R$ at $f_{\text{RH}-1\text{FD}}$.

D. METALPA$_O$ OF A CIRCUMFERENCE OF TWO GUIDED WAVELENGTHS (STEP FOUR)

Fig. 14 shows a metaloop antenna composed of C-type metaatoms, where F_O denotes the feed point and T_O denotes the terminal point, which is short-circuited to the ground plane through resistive load R_B (= 50 ohms). The loop circumference is two guided wavelengths ($2\lambda_g$) at $f_{\text{LH}-1\text{FD}} = 2.55$ GHz and $f_{\text{RH}-1\text{FD}} = 3.45$ GHz. The diameter of the grounded dielectric substrate is the same as that for the 1FD-MetaLPA: $0.72\lambda_g$ at $f_{\text{LH}-1\text{FD}}$. Other parameters are the same as those shown in Table 1. This metaloop antenna is denoted as the MetaLPA$_O$.

Representative radiation patterns are shown in Fig. 15. It is found that a conical radiation pattern is formed with principal field component E_L below transition frequency f_T and principal field component E_R above f_T. The phase progressions for

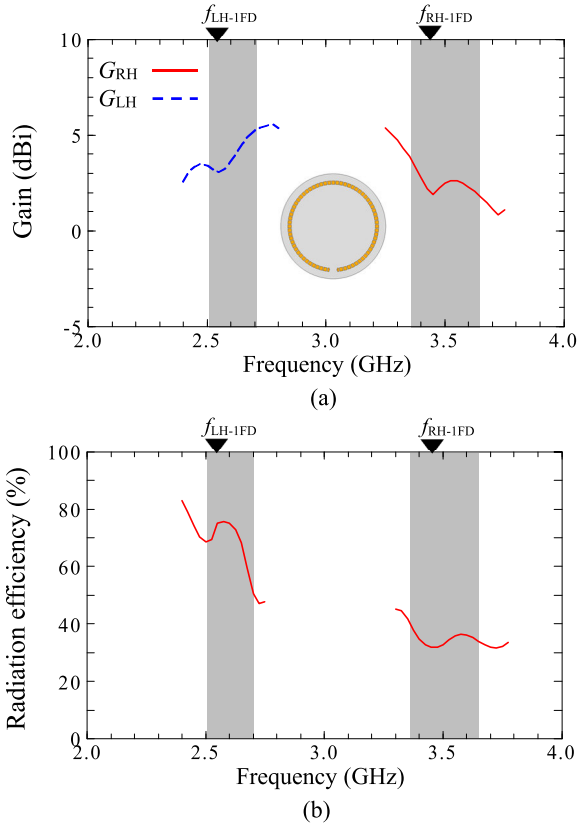

FIGURE 17. Frequency response. (a) Gain in the direction of maximum radiation for the MetaLPA$_O$. For comparison, the shaded areas show the 3-dB gain bandwidth regions for the 1FD-MeraLPA in Fig. 11(a). (b) Radiation efficiency.

E_L at f_{LH-1FD} (= 2.55 GHz) and E_R at f_{RH-1FD} (= 3.45 GHz) as a function of azimuth angle ϕ are shown in Fig. 16, where a phase change of 720° is obtained.

Fig. 17(a) shows the frequency response around frequencies f_{LH-1FD} and f_{RH-1FD} with respect to the gain in the direction of maximum radiation. For comparison, the 3-dB gain bandwidth regions for the gain-balanced 1FD-MetaLPA, *i.e.*, the shaded regions in Fig. 11(a), are also shown. It is found that the difference between the gain at f_{LH-1FD} and the gain at f_{RH-1FD} is small. The radiation efficiency is 75% at f_{LH-1FD} and 32% at f_{RH-1FD}, as shown in Fig. 17(b). Note that the VSWR across the shaded regions is small, with a value of less than two, as is observed for the gain-balanced 1FD-MetaLPA (not shown).

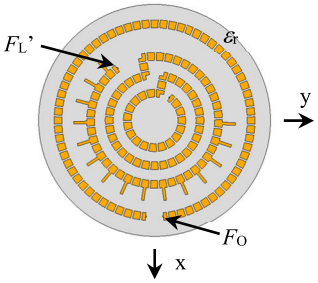

FIGURE 18. MetaLPA-plus with two feed points, F_L' and F_O.

E. COMPOUND OF THE GAIN-BALANCED 1FD-METALPA AND METALPA$_O$ (STEP FIVE)

To form a tilted beam, a compound of the gain-balanced 1FD-MetaLPA and MetaLPA$_O$, designated as the MetaLPA- plus, is investigated. The MetaLPA-plus, shown in Fig. 18, has two feed points, F_L' and F_O. These feed points are, respectively, excited by voltages V_L and V_O with equal amplitude.

$$V_L = A\angle\Phi_L \tag{1}$$
$$V_O = A\angle\Phi_O \tag{2}$$

where A and $\angle\Phi_i$ (i = L, O) are the amplitude and phase, respectively, and $\Delta\Phi$ is the phase that is relative to $\angle\Phi_L$: $\Delta\Phi \equiv \angle\Phi_O - \angle\Phi_L$.

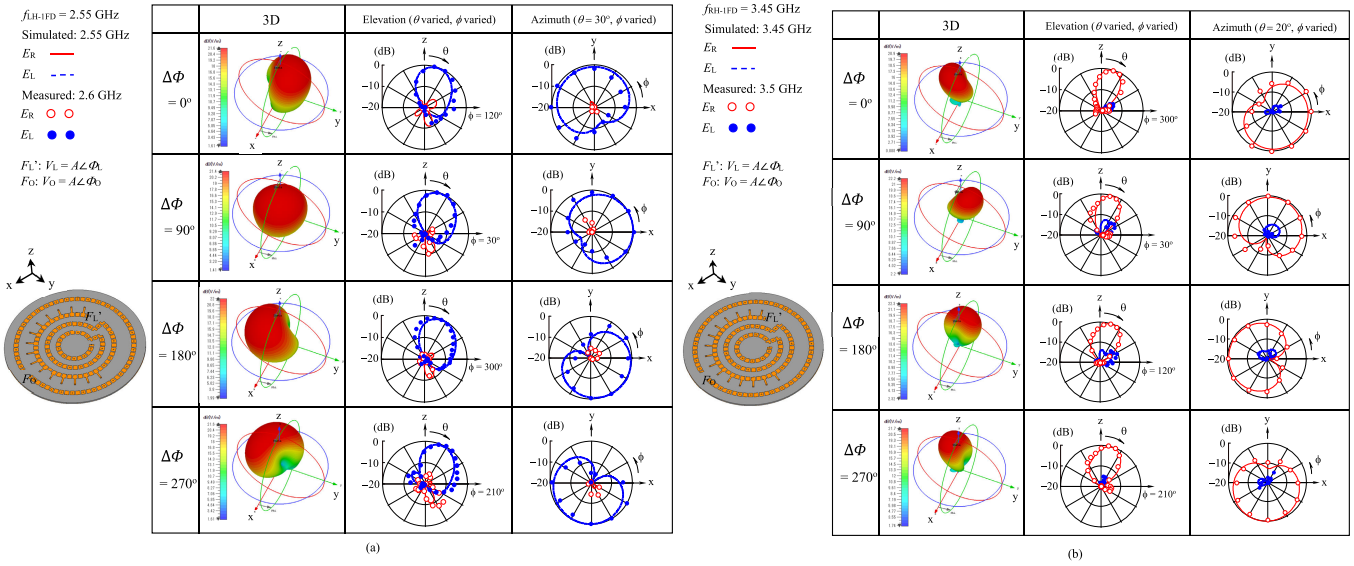

FIGURE 19. Movement of the tilted beam for the MetaLPA-plus. (a) At f_{LH-1FD}. (b) At f_{RH-1FD}.

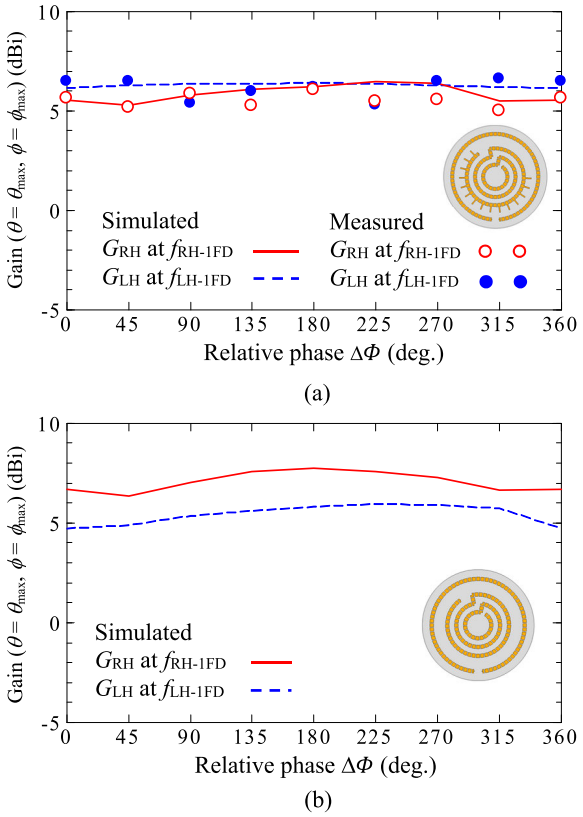

FIGURE 20. Maximum gains G_{LH} at f_{LH-1FD} and G_{RH} at f_{RH-1FD} as a function of relative phase $\Delta\Phi$. (a) MetaLPA-plus, composed of the gain-balanced 1FD-MetaLPA and MetaLPA$_O$. (b) Antenna composed of the gain-unbalanced 1FD-MetaLPA in Fig. 5 and MetaLPA$_O$.

The radiation field from the compound MetaLPA-plus is the sum of the axial beam from the gain-balanced 1FD-MetaLPA and the conical beam from the MetaLPA$_O$. Overlapping of the two beams forms a tilted beam, whose direction is denoted as $(\theta, \phi) = (\theta_{max}, \phi_{max})$. The polarization of the tilted beam is LHCP at frequency f_{LH-1FD} due to a negative β and RHCP at f_{RH-1FD} due to a positive β.

Fig. 19 shows the simulated movement of the tilted beam when relative phase $\Delta\Phi$ is changed. It is found that the tilted beam rotates around the z-axis in a clockwise direction (Fig. 19(a)) and a counterclockwise direction (Fig. 19(b)). The azimuth angle of the beam direction for $\Delta\Phi = 0°$ at f_{LH-1FD}, denoted as $\phi_{LH-CPmax-0}$, is determined by the intersection point of the lines in Figs. 13(a) and 16(a): $\phi_{LH-CPmax-0} \approx 120°$. Similarly, the azimuth angle of the beam direction for $\Delta\Phi = 0°$ at f_{RH-1FD}, denoted as $\phi_{RH-CPmax-0}$, is determined by the intersection point of the lines in Figs. 13(b) and 16(b): $\phi_{RH-CPmax-0} \approx 300°$.

Note that beam direction coordinate θ_{max} at $\phi_{LH-CPmax-0}$ is found from the summation of $E_L(\theta, \phi = \phi_{LH-CPmax-0})$ for the axial beam and $E_L(\theta, \phi = \phi_{LH-CPmax-0})$ for the conical beam: $\theta_{max} = 20°$. In addition, θ_{max} at $\phi_{RH-CPmax-0}$ is found from the summation of $E_R(\theta, \phi = \phi_{RH-CPmax-0})$ for the axial beam and $E_R(\theta, \phi = \phi_{RH-CPmax-0})$ for the conical beam: $\theta_{max} = 15°$. These θ_{max} values remain almost unchanged with variation in relative phase $\Delta\Phi$. Note that the axial ratio bandwidth for $\Delta\Phi = 0°$ is approximately 8% around both f_{LH-1FD} and f_{RH-1FD}.

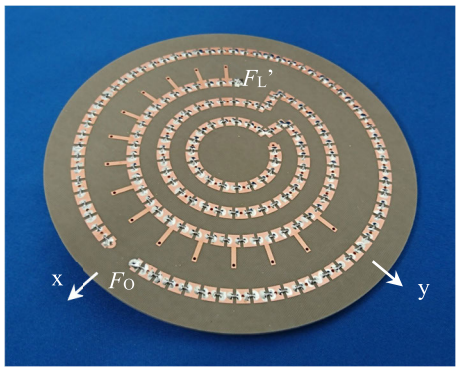

FIGURE 21. Fabricated MetaLPA-plus.

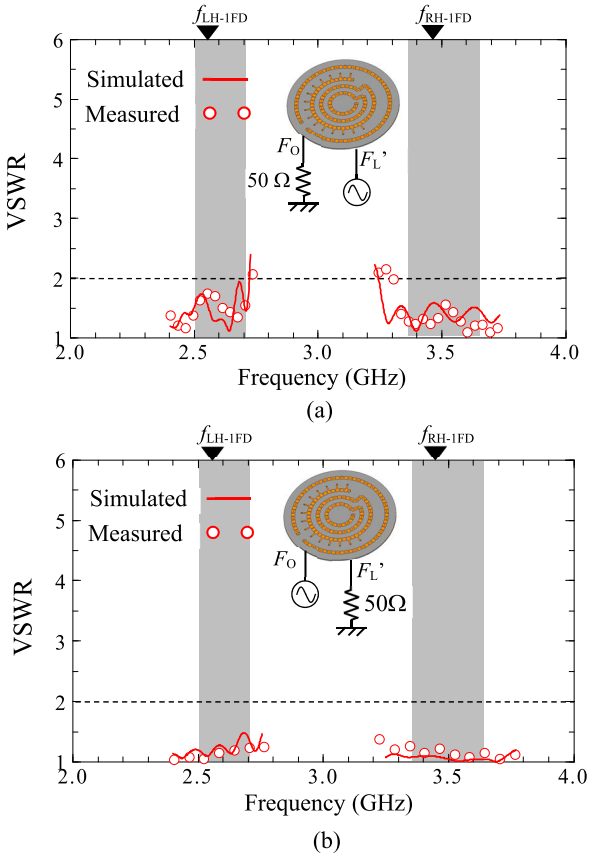

FIGURE 22. Frequency response of the VSWR for the MetaLPA-plus. (a) Excitation at F_L' for the inner gain-balanced 1FD-MetaLPA. (b) Excitation at F_O for the outer MetaLPA$_O$.

Fig. 20(a) shows the maximum gain for the MetaLPA-plus as a function of $\Delta\Phi$. The difference between G_{LH} at f_{LH-1FD} and G_{RH} at f_{RH-1FD} is small due to the almost unchanging radiation pattern in the azimuth and elevation directions, as shown in Fig. 19. For comparison, Fig. 20(b) shows the maximum gain for an antenna system composed of the 1FD-MetaLPA and MetaLPA$_O$, where G_{LH} and G_{RH} for the 1FD-MetaLPA are unbalanced, as shown in Fig. 6.

TABLE 3. Comparison of the MetaLPA-plus with other published CP beam-steering antennas.

	Height	Band	Polarization	Number of feed points	Impedance bandwidth	AR bandwidth	Continuous steering ability
MetaLPA-plus	$0.014\lambda_0$	Dual	LHCP and RHCP	2	>10%	≈8%	Yes
[14]	$0.197\lambda_0$	Single	RHCP	4	16.6%	10.7%	No
[15]	$0.026\lambda_0$	Single	LHCP	4	>10%	19%	No
[16]	$0.068\lambda_0$	Single	RHCP	2	5.1%	1.4%	Yes
[17]	$0.017\lambda_0$	Single	RHCP	4	1.4%	Not clear	Yes
[18]	$0.013\lambda_0$	Single	LHCP	2	Not clear	Not clear	Yes
[19]	$0.008\lambda_0$	Single	LHCP or RHCP	4	≈1%	≈1%	Yes
[20]	$0.46\lambda_0$	Single	RHCP	1	67%	47%	No

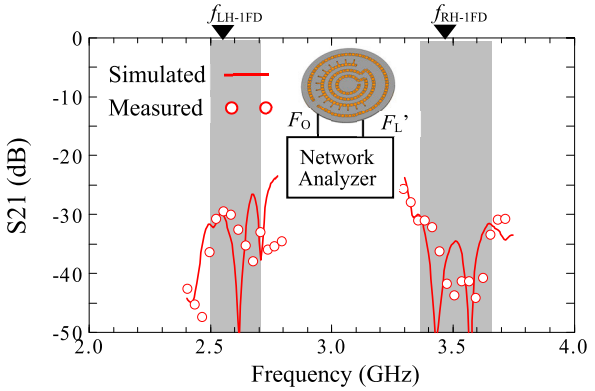

FIGURE 23. Mutual coupling between feed points F_L' and F_O.

III. RESULTS AND DISCUSSION

To confirm the beam rotation discussed in Subsection E of Section II, a MetaLPA-plus is fabricated, as shown in Fig. 21, using the parameters in Tables 1 and 2, where the inner gain-balanced 1FD-MetaLPA has a radius of 41.8 mm and the outer MetaLPA_O has a radius of 54.1 mm.

The measured 2D radiation pattern results for the MetaLPA-plus are shown in Fig. 19 together with the simulated results. It is found that the measured results, observed at frequencies very close to f_{LH-1FD} and f_{RH-1FD}, confirm the rotation of the simulated radiation beam with change in relative phase $\Delta\Phi$. Fig. 20(a) shows the measured and simulated maximum gains as a function of $\Delta\Phi$, which are found to be almost the same.

Fig. 22 shows the measured VSWR. It is found that the VSWR is desirably small across the 3-dB gain bandwidth defined in Fig. 11. Fig. 23 depicts the mutual coupling between feed points F_L' and F_O (S21). The mutual coupling is very small: less than −25 dB. The radiation efficiency of the inner gain-balanced 1FD-MetaLPA is 72% at f_{LH-1FD} and 28% at f_{RH-1FD}. On the other hand, the radiation efficiency of the outer MetaLPA_O is 63% at f_{LH-1FD} and 22% at f_{RH-1FD}.

IV. CONCLUSION

A counter circularly polarized (CP) dual-band MetaLPA-plus with a tilted beam has been designed and the radiation characteristics have been revealed. Investigation starts with a CP antenna system with three feed points, the 3FD- MetaLPA, which is composed of three metaloop antennas, the MetaLPA_L, MetaLPA_M, and MetaLPA_S. It is found that the 3FD-MetaLPA with in-phase excitation of the three feed points has a maximum gain which is slightly larger than that for the single MetaLPA_M whose circumference is approximately 0.9 guided wavelength. Based on the results for the 3FD-MetaLPA, a 1FD-MetaLPA with a single feed point is formed and investigated, where the three metaloops for the 3FD-MetaLPA are connected such that they share a single feed point. It is revealed that the 1FD-MetaLPA has a larger gain than the 3FD-MetaLPA. It is also revealed that the maximum gain for a left-hand circularly polarized (LHCP) wave at low frequency f_{LH-1FD} and the maximum gain for a right-hand circularly polarized (RHCP) wave at high frequency f_{RH-1FD} are not balanced. Subsequently, these unbalanced gains are balanced using N-type metaatoms. The 1FD-MetaLPA with balanced gain radiates an axial beam. The gain bandwidth for a left-hand CP wave is 7.7% with a maximum gain value of 7.1 dBi. The gain bandwidth for a right-hand CP wave is 8.3% with a maximum gain value of 7.1 dBi. The VSWR across these gain bandwidths is smaller than two, as desired.

Lastly, a large metaloop antenna that radiates a conical beam and has a feed point, F_O, is concentrically added to the outside of the gain-balanced 1FD-MetaLPA. This compound antenna is designated as the MetaLPA-plus. When the outer MetaLPA_O and inner gain-balanced 1FD-MetaLPA are excited with equal amplitude, the MetaLPA-plus forms

a tilted CP beam. It is found that the tilted CP beam can be rotated around the antenna axis (z-axis) by changing the excitation phase for the MetaLPA-plus.

APPENDIX

Table 3 shows comparison of the MetaLPA-plus with other published CP beam-steering antennas.

ACKNOWLEDGMENT

The authors thank V. Shkawrytko for his assistance in the preparation of this manuscript.

REFERENCES

[1] P. J. Massey, P. Fellows, D. Mirshekar-Syahkal, A. Pal, and A. Mehta, "Loop antennas," in *Handbook of Antenna Technologies*, vol. 2. Cham, Switzerland: Springer, 2016, pp. 723–786.

[2] C. Balanis, *Antennas Theory*. Hoboken, NJ, USA: Wiley, 2005, ch. 5.

[3] H. Nakano, "A numerical approach to line antennas printed on dielectric materials," *Comput. Phys. Commun.*, vol. 68, nos. 1–3, pp. 441–450, Nov. 1991.

[4] K. Hirose, Y. Kikkawa, and H. Nakano, "Decoupling and sequential array antennas—Effects of coplanar feedline on radiation characteristics," *IEEE Antennas Wireless Propag. Lett.*, vol. 19, no. 3, pp. 423–427, Mar. 2020.

[5] K. Hirose, T. Shibasaki, Y. Yoshida, and H. Nakano, "Ladder antennas for dual circular polarization," *IEEE Antennas Wireless Propag. Lett.*, vol. 11, pp. 1174–1177, 2012.

[6] C. Caloz and T. Itoh, *Electromagnetic Metamaterials*. Hoboken, NJ, USA: Wiley, 2006.

[7] J.-H. Park, Y.-H. Ryu, J.-G. Lee, and J.-H. Lee, "Epsilon negative zeroth-order resonator antenna," *IEEE Trans. Antennas Propag.*, vol. 55, no. 12, pp. 3710–3712, Dec. 2007.

[8] J. K. Ji, G. H. Kim, and W. M. Seong, "Bandwidth enhancement of metamaterial antennas based on composite right/left-handed transmission line," *IEEE Antennas Wireless Propag. Lett.*, vol. 9, pp. 36–39, 2010.

[9] A. Lakhtakia and C. Furse, Eds., *The World of Applied Electromagnetics*. Cham, Switzerland: Springer, 2018, ch. 7.

[10] H. Nakano, K. Sakata, and J. Yamauchi, "Linearly and circularly polarized radiation from metaline antennas," in *Proc. Int. Workshop Antenna Technol. (iWAT)*, Cocoa Beach, FL, USA, Feb. 2016, pp. 142–143.

[11] H. Nakano, K. Yoshida, and J. Yamauchi, "Radiation characteristics of a metaloop antenna," *IEEE Antennas Wireless Propag. Lett.*, vol. 12, pp. 861–863, 2013.

[12] H. Nakano, T. Abe, and J. Yamauchi, "Quasi-theoretical investigation of four circularly polarized metaloop antennas," *Eur. Phys. J. Appl. Metamaterials*, vol. 6, no. 2, pp. 1–13, Jan. 2019.

[13] CST Computer Simulation Technology GmbH, Darmstadt, Germany. *Microwave Studio*. Accessed: Dec. 2020. [Online]. Available: http://www.cst.com

[14] H. Zhou, A. Pal, A. Mehta, D. Mirshekar-Syahkal, and H. Nakano, "A four-arm circularly polarized high-gain high-tilt beam curl antenna for beam steering applications," *IEEE Antennas Wireless Propag. Lett.*, vol. 17, no. 6, pp. 1034–1038, Jun. 2018.

[15] H. Nakano, T. Abe, and J. Yamauchi, "Planar reconfigurable antennas using circularly polarized metalines," *IEEE Antennas Wireless Propag. Lett.*, vol. 18, no. 5, pp. 1006–1010, May 2019.

[16] C. Deng, Y. Li, Z. Zhang, and Z. Feng, "A hemispherical 3-D null steering antenna for circular polarization," *IEEE Antennas Wireless Propag. Lett.*, vol. 14, pp. 803–806, 2015.

[17] N. R. Labadie, S. K. Sharma, and G. M. Rebeiz, "A circularly polarized multiple radiating mode microstrip antenna for satellite receive applications," *IEEE Trans. Antennas Propag.*, vol. 62, no. 7, pp. 3490–3500, Jul. 2014.

[18] H. Nakano, T. Abe, T. Kawano, A. Mehta, and J. Yamauchi, "Azimuth angle estimation for a reduced radiation region formed by a metaspiral antenna," *IEEE Access*, vol. 7, pp. 78289–78297, Jun. 2019.

[19] M. Barbuto, A. Alu, F. Bilotti, and A. Toscano, "Dual-circularly polarized topological patch antenna with pattern diversity," *IEEE Access*, vol. 9, pp. 48769–48776, Mar. 2021.

[20] L. Ge, M. Li, Y. Li, H. Wong, and K.-M. Luk, "Linearly polarized and circularly polarized wideband dipole antennas with reconfigurable beam direction," *IEEE Trans. Antennas Propag.*, vol. 66, no. 4, pp. 1747–1755, Apr. 2018.

HISAMATSU NAKANO (Life Fellow, IEEE) has been with Hosei University, since 1973, where he is currently a Professor Emeritus and a Special-appointment Researcher with the Electromagnetic Wave Engineering Research Institute attached to the Graduate School. He has held positions as a Visiting Associate Professor with Syracuse University, from March 1981 to September 1981, and a Visiting Professor with the University of Manitoba, from 1986 March to September 1986, the University of California at Los Angeles, Los Angeles, from September 1986 to March 1987, and Swansea University, U.K., from July 2016 to September to 2019. His significant contributions are the development of five integral equations for line antennas in free space and printed on a dielectric substrate, the invention of an L-shaped wire/strip antenna feeding method, and the realization of numerous wideband antennas, including curl, metaspiral, metahelical, and body of revolution antennas. His other accomplishments include design of antennas for GPS, personal handy phones, space radio, electronic toll collection, RFID, UWB, and radar. He has published over 330 articles in peer-reviewed journals and 11 books/book chapters, including *Low-profile Natural and Metamaterial Antennas* (Wiley-IEEE Press, 2016). His research interests include numerical methods for low-frequency antennas and high-frequency antennas and optical waveguides. He served as a member for the IEEE APS Administrative Committee, from 2000 to 2002, and a Region Ten Representative, from 2001 to 2010. He received the H. A. Wheeler Award, in 1994, the Chen-To Tai Distinguished Educator Award, in 2006, and the Distinguished Achievement Award, in 2016, all from the IEEE Antennas and Propagation Society. He was also a recipient of the Prize for Science and Technology from Japan's Ministry of Education, Culture, Sports, Science and Technology, in 2010. Most recently, he was selected as a recipient of the Antenna Award of the *European Association on Antennas and Propagation (EurAAP)*, in 2020. He has been awarded 78 patents, including *A Curl Antenna Element and Its Array*, Japan. He is an Associate Editor of several scientific journals and magazines, including *Electromagnetics*.

TOMOKI ABE (Member, IEEE) was born in Miyagi, Japan, in August 1994. He received the B.E. and M.E. degrees in electronics and electrical engineering from Hosei University, Tokyo, Japan, in 2017 and 2019, respectively. He is currently a graduate student of doctoral course at Hosei University.

JUNJI YAMAUCHI (Life Fellow, IEEE) was born in Nagoya, Japan, in August 1953. He received the B.E., M.E., and Dr.Eng. degrees from Hosei University, Tokyo, Japan, in 1976, 1978, and 1982, respectively. From 1984 to 1988, he served as a Lecturer for the Department of Electrical Engineering, Tokyo Metropolitan Technical College. Since 1988, he has been a member of the Faculty of Hosei University, where he is currently a Professor with the Department of Electrical and Electronic Engineering. He has authored *Propagating Beam Analysis of Optical Waveguides* (Research Studies Press, 2003). His research interests include optical waveguides, polarization converters, and circularly polarized antennas. He is a member of the Optical Society of America and the Institute of Electronics, Information and Communication Engineers of Japan.